Supporting Information

Label-free, real-time monitoring of membrane binding events at zeptomolar concentrations using frequency-locked optical microresonators

Adley Gin[1*], Phuong-Diem Nguyen[2*], Jeffrey Melzer[1], Cheng Li[1], Hannah Strzelinski[3], Stephen B. Liggett[3], and Judith Su[1,2**]

[1]Wyant College of Optical Sciences, The University of Arizona, Tucson, AZ 85721, USA
[2]Department of Biomedical Engineering, The University of Arizona, Tucson, AZ 85721, USA
3Department of Medicine, University of South Florida Morsani College of Medicine, Tampa, FL 33612, USA

*These authors contributed equally to this work.

**Address correspondence to: judy@optics.arizona.edu

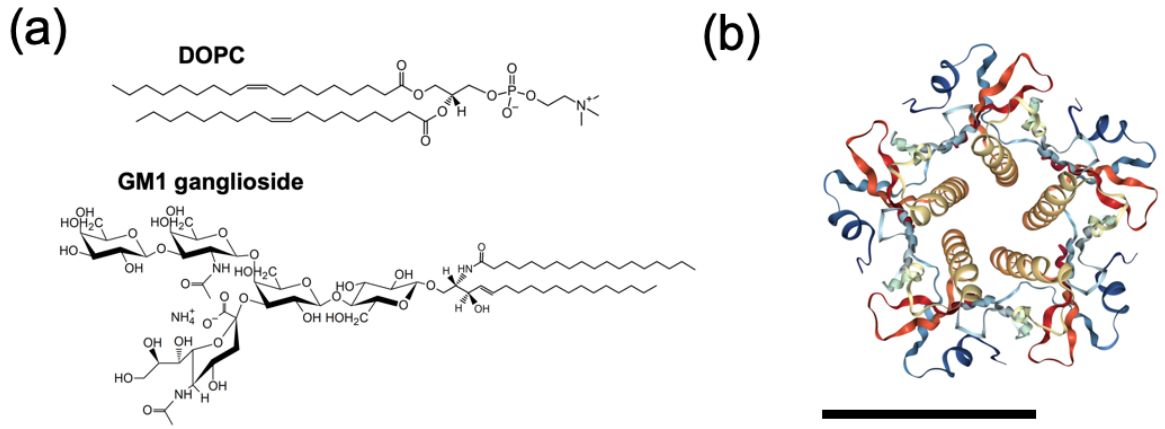

Fig. S1. Chemical structures of lipid, receptor, and cholera toxin B. (a) Chemical structure of the DOPC lipid and GM1 receptor glycolipid investigated in this study. (b) Pentameric structure of the cholera toxin B-subunit (Image from RCSB PDB (rcsb.org) of 1FGB (Zhang, R.G., Westbrook, M.L., Westbrook, E.M., Scott, D.L., Otwinowski, Z., Maulik, P.R., Reed, R.A., Shipley, G.G. (1995). The 2.4 Å crystal structure of cholera toxin B subunit pentamer: choleragenoid. J.Mol.Biol. 251: 550-562). The scale bar is 3.6 nm.

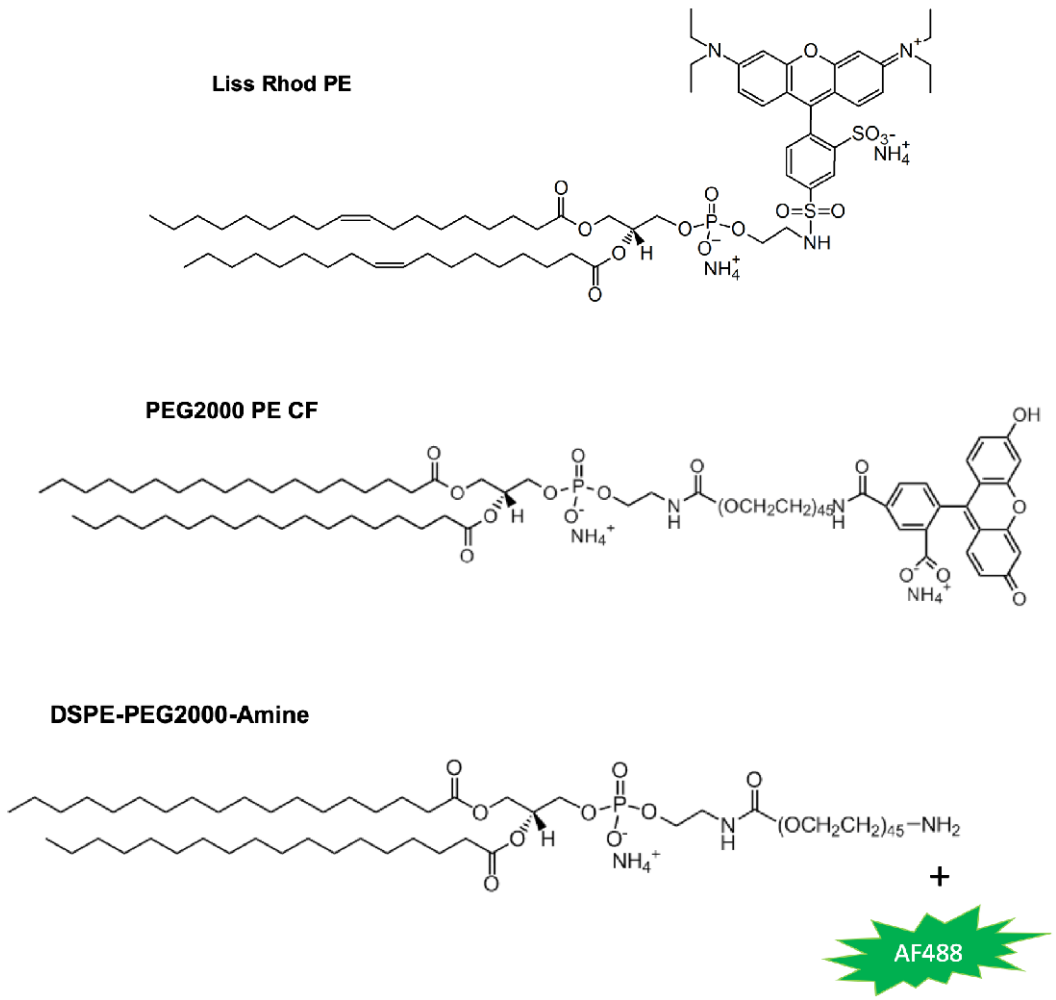

Fig. S2. Chemical structures of fluorescently labeled lipids used in this study. For the FRAP experiments, DSPE-PEG2000-Amine labeled with AF488 NHS ester was used to achieve better photostability than 18:1 PE CF (1,2-dioleoyl-sn-glycero-3-phosphoethanolamine-N-(carboxyfluorescein)).

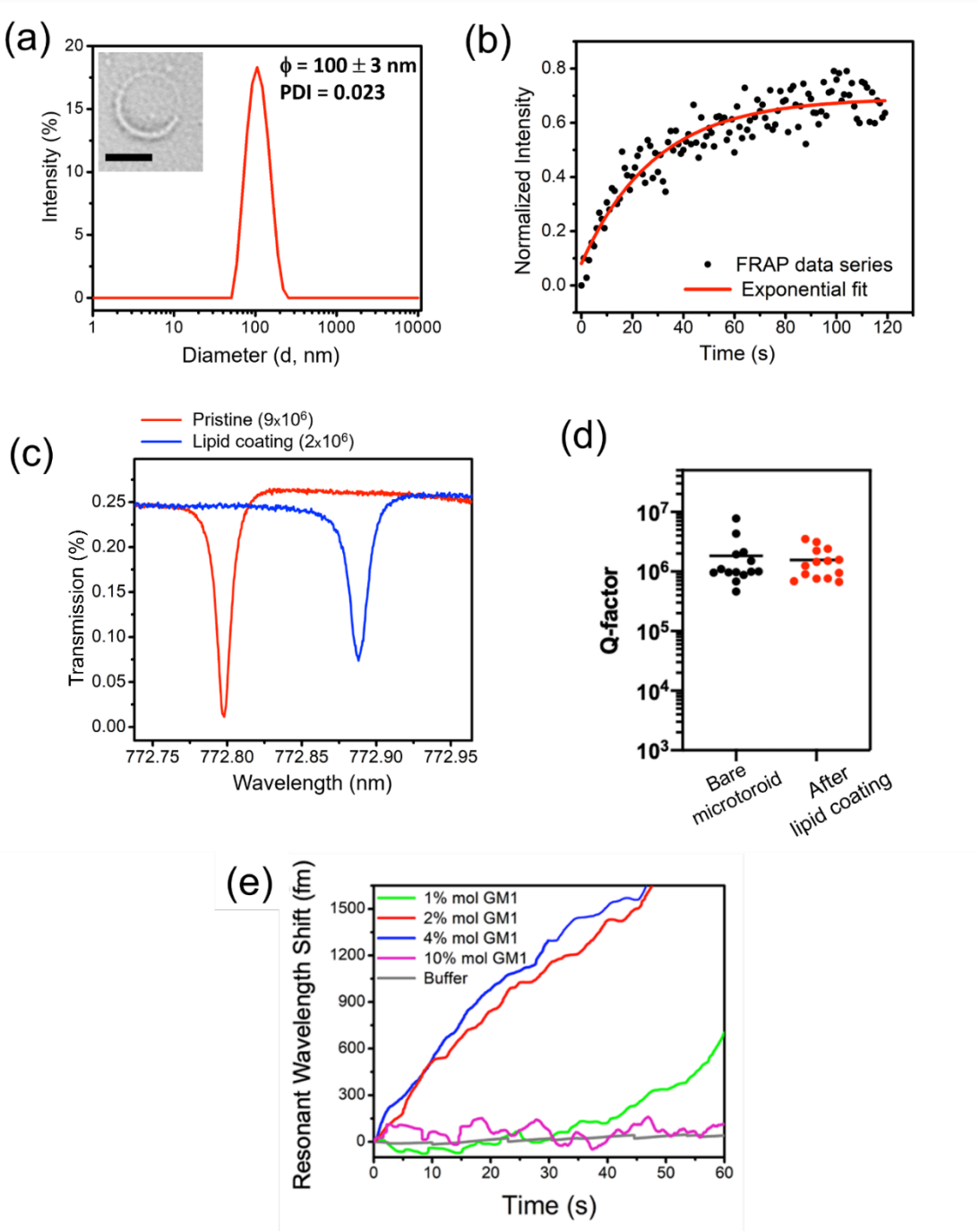

Fig. S3. Coating microtoroids with GM1-DOPC lipids. (a) Dynamic light scattering (DLS) measurement of GM1-DOPC lipid vesicles, showing a narrow size distribution centered at 100 nm. The inset picture is a TEM image of GM-DOPC lipid vesicles revealed by uranyl acetate staining (scale bar 50 nm). (b) FRAP experiment showing the fluorescence recovery of the lipid supported microtoroid. (c, d) Quality (Q)-factor measurement of microtoroid optical resonators before and after lipid coating (all the measurements were done in aqueous condition, recorded from different microtoroids on different days of experiments (n=14). Center line shows the mean of the data. (e) Resonant wavelength shift data as 1 nM CTB was injected for different %mol doped GM1-DOPC lipid coated microtoroids

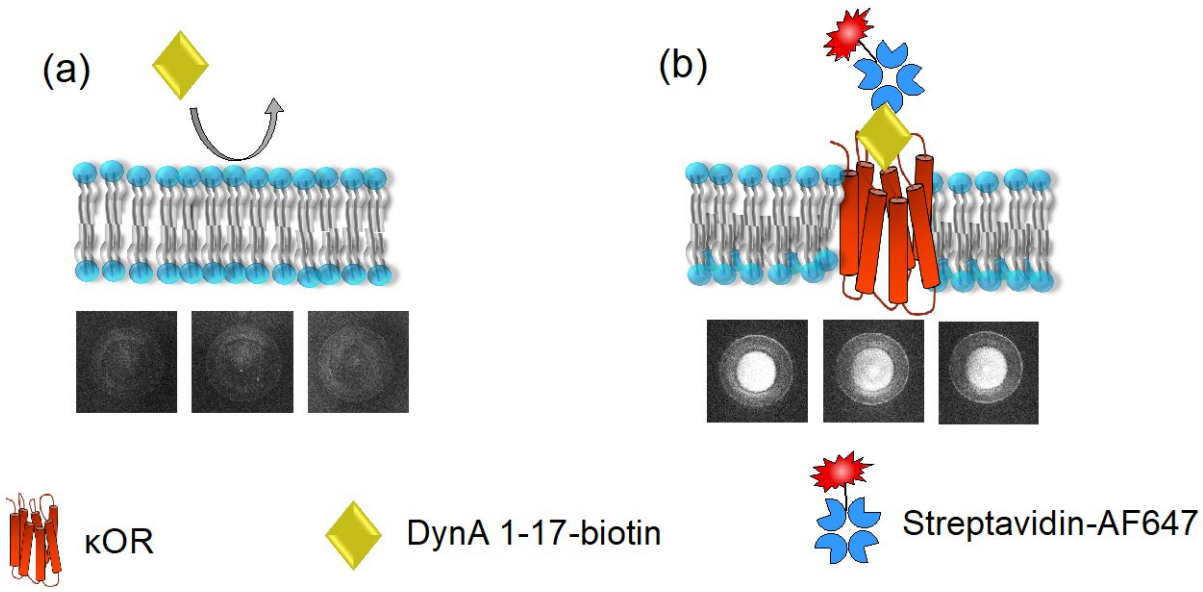

Fig. S4. Fluorescent imaging experiment to confirm the specificity of biotin DynA 1-17 to κOR reconstituted lipid coated microtoroid sensors. The fluorescent label used is streptavidin-AF647. (a) Control experiment of DynA 1-17 binding to a κOR-free, lipid-coated microtoroid sensor. As expected, little binding is observed. (b) DynA 1-17-streptavidin binding to a κOR reconstituted lipid coated microtoroid sensor. A bright fluorescence was revealed.

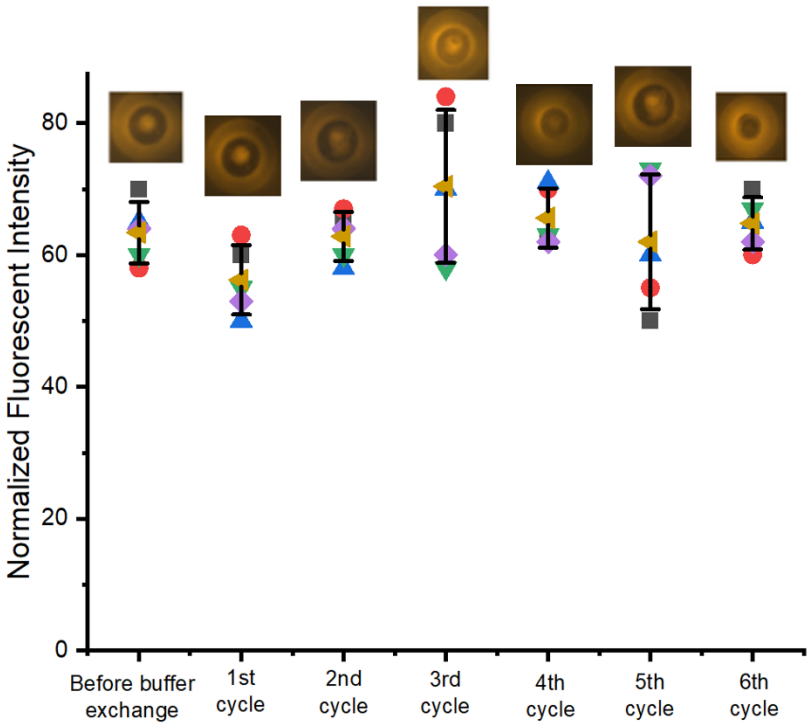

Fig. S5. Lipid functionalization stability during several cycles of complete buffer exchange (Tris 25 mM, NaCl 150 mM, pH 7.4). Liss Rhod PE doped DOPC lipid was used in this experiment. The average fluorescent intensity was taken from 3 random microtoroids on one chip. Bars and whiskers show mean ± SEM of the data. The fluorescence was normalized to the background intensity.

Investigation of GM1-CTB toroid surface regeneration. To achieve a high-throughput study for measuring GM1-CTB interactions using the microtoroid sensor, the CTB saturated surface was regenerated using a regeneration solution known to disrupt the interaction of CTB to GM1 receptors (i.e. 6M Urea, 25 mM Glycine, 160 mM NaCl, pH 2.5).[71] The regeneration efficiency was confirmed by a fluorescent imaging assay. CTB labeled with AF647 was bound to a GM1-DOPC membrane labeled with carboxyfluorescein (PEG2000 PE CF). The decrease in AF647 after regeneration is directly related to the restored GM1 binding sites. As expected, after introducing the regeneration solution, the fluorescence intensity from CTB-AF647 significantly decreased while the fluorescence from the lipid membrane remained (Fig. S5). After 10 cycles of regeneration (by complete buffer exchange, Fig. S5), the CTB binding capacity still sufficiently remained. The regeneration efficiency was not significantly different between 2 consecutive cycles (2 min per cycle). The optimal regeneration time was 2 minutes. Each regeneration cycle was followed by binding buffer wash supplemented with 0.5% BSA to prevent non-specific binding which may result from unexpected lipid removal.

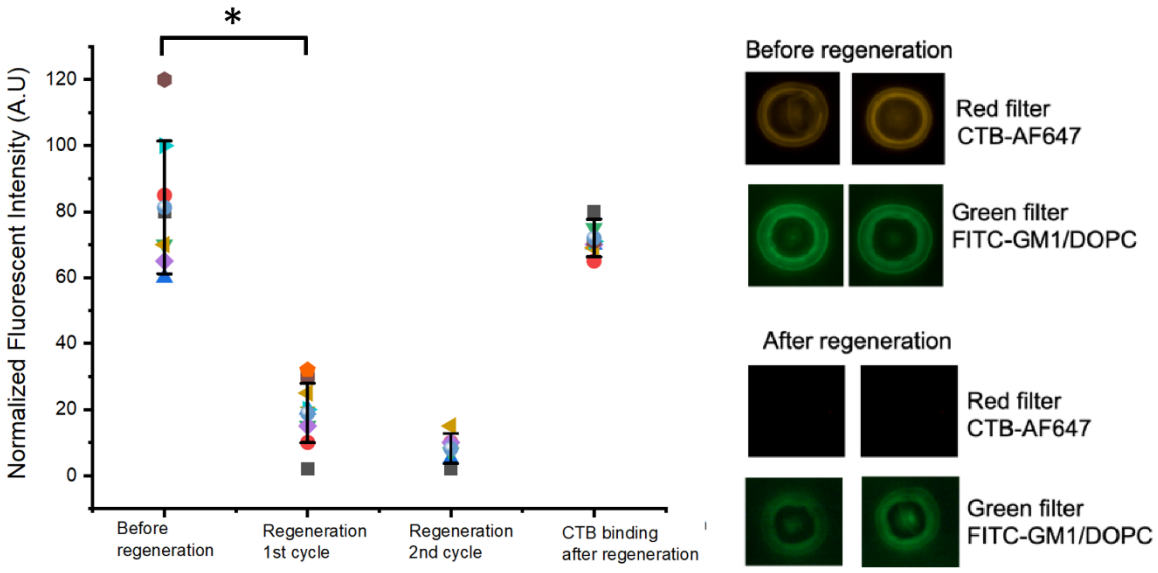

Fig. S6. CTB-GM1 regeneration using regeneration buffer (glycine 25 mM, Urea 6 M, NaCl 0.1 M, pH 3) characterized by fluorescent imaging (a) Plot of normalized fluorescent intensity of CTB-AF647 binding to a GM1-DOPC coated microtoroid before and after a regeneration step (statistical evidence $*p < 0.05$ performed by one-way ANOVA, n = 6). Bars and whiskers show the mean ± SEM of the data. No significant difference in regeneration efficiency was observed between the two washes (2 mins each). The GM1-DOPC binding efficacy is high even after 10 regeneration cycles on-chip, (b) Corresponding fluorescent intensity images of CTB-AF647 binding to a GM1-DOPC supported microtoroid surface. The red fluorescence is from CTB-AF647 and the green fluorescence is from FITC labeled GM1-DOPC. Fluorescence imaging was performed for visualization of the retained lipid membrane after regeneration (FITC labeled GM1-DOPC intensity data was normalized with the images taken in the binding buffer (Tris 25 umM, NaCl 150 mM) only).

Direct deposition of κOR membrane vs. κOR reconstitution. The κOR/DynA pharmacokinetic study requires the surface of the silica toroid sensor to be functionalized with the receptors embedded in a lipid membrane. HEK-293T+ κOR cells were suspended in buffer and mechanically disrupted with a syringe and needle. We initially tried incubating the toroid sensors in a solution of crude HEK-293T cell membrane fragments containing κOR directly on the toroid. However, the toroid Q-factor was degraded significantly because natural cell membranes contain many other additional proteins besides our protein of interest as well as larger cell fragments contributing to increased surface roughness and scattering loss. To maintain high Q factors, we instead remove the κOR from the crude cell membrane by detergent solubilization and reconstitute it in an artificial DOPC lipid bilayer.[1] This has the added benefit of dispersing the GPCRs, which can be tightly packed in a natural membrane, restricting ligand access to binding sites. Therefore, our approach *extends,* rather than restricts, general applicability. In general, an engineered membrane-receptor system has the potential for wider applicability than a natural-receptor system. For our other reported experiments (cholera toxin B binding to GM1), we obtained the GM1 in purified form and did not need to extract it from a natural membrane, and so there was no Q factor degradation in those experiments either.

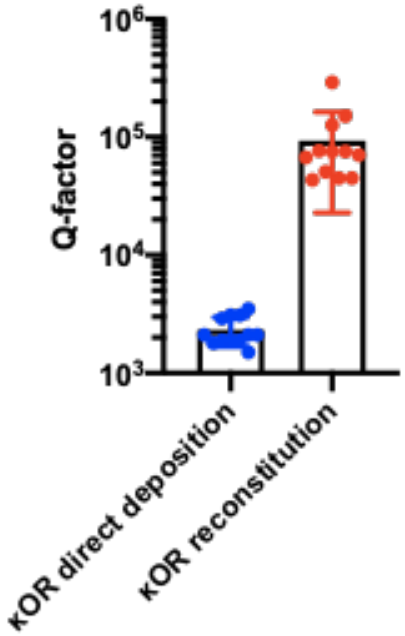

Fig. S7. Quality (Q)-factor data showing Q degradation when using direct deposition of a crude cell membrane (n = 12) vs reconstitution of κOR in a lipid bilayer (n = 12). Bars and whiskers show the mean ± SEM of the data. Direct deposition of κOR-proteolipid membrane degrades the microtoroid quality factor because the cell membrane contains many other additional proteins besides our protein of interest. For our sensor system, we achieve higher quality factors if we remove the κOR from the crude cell membrane and reconstitute it in a lipid bilayer. Tightly packed GPCRs restrict access to binding sites[2]; this is avoided if we reconstitute the proteins in a lipid bilayer.

Experimental Setup.

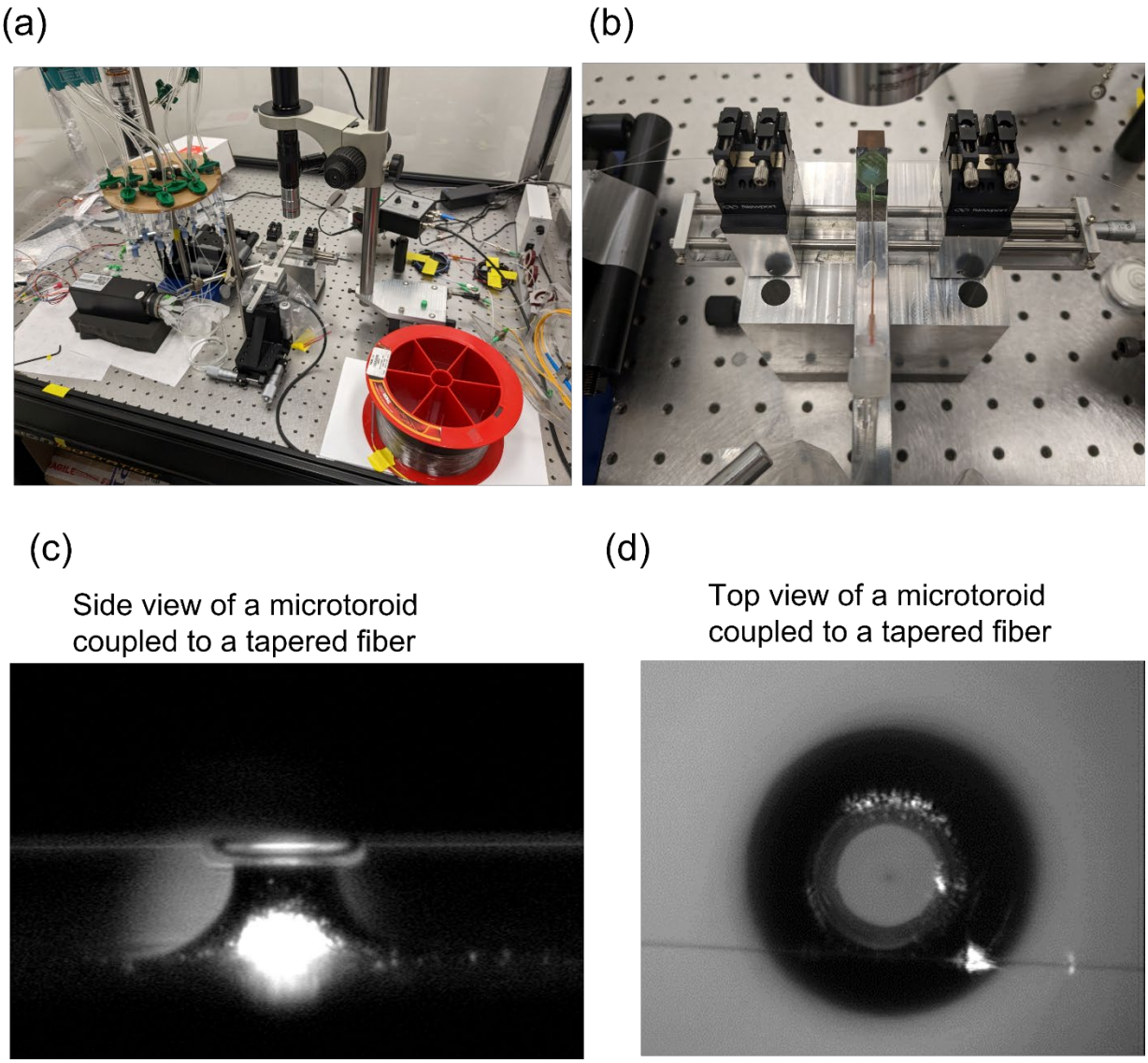

Fig. S8. Experimental setup and view of microtoroid and tapered fiber. (a) Experimental setup of FLOWER system: pressurized perfusion system and rotary valve for delivering fluid samples (left). Top-view microscope, fluidic chamber, tapered fiber stage, and piezoelectric nano-positioning cube on a 3-axis micrometer stage (middle). Single-mode fiber spool, in-line polarizer, attenuator, and photodetector (right). (b) Closer view of the fluidic chamber (green) positioned in the tapered fiber stage, along with the perfusion needle which delivers liquid samples into the fluidic chamber. (c) Side view of microtoroid and tapered fiber. (d) Top view of the microtoroid coupled to a tapered fiber.

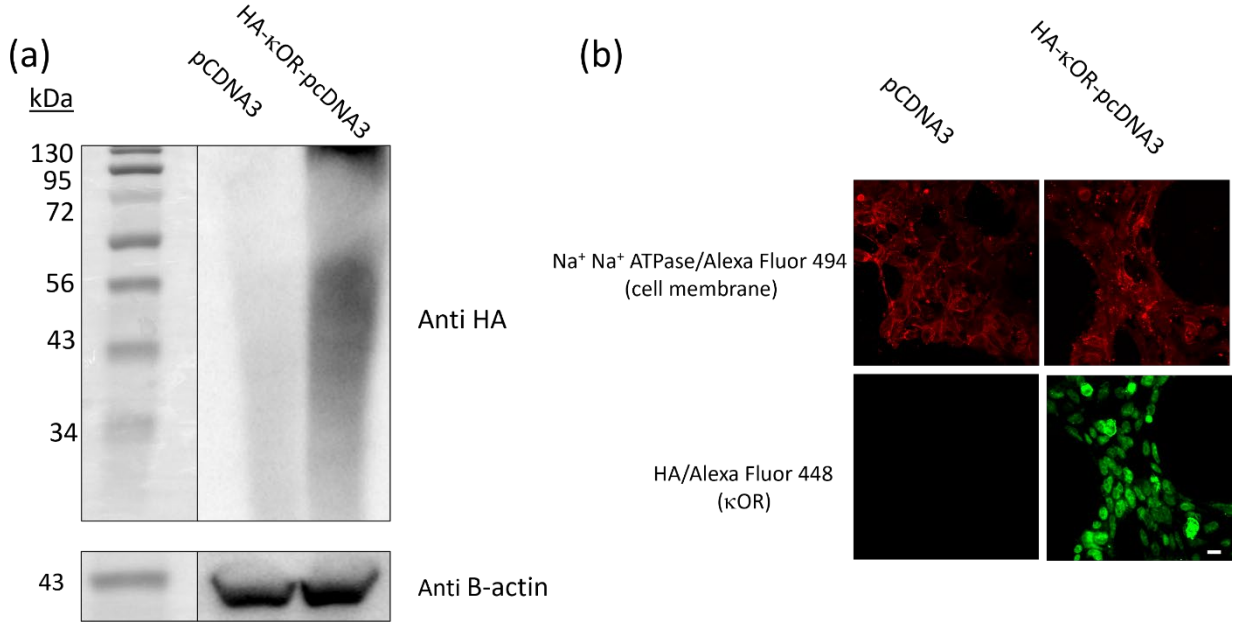

Fig. S9. Expression of κOR in HEK-293T cells. (a) Immunoblot of cell lysates showing expression of κOR only from the cells transfected with the HA-κOR-pcDNA3 expression vector. (b) Confocal microscopy of nonpermeabilized HEK-293T transfected with empty vector or the κOR expression vector. Red = cell membrane from incubation with Na+ K+ ATPase conjugated to Alexa Fluor 594. Green = expression of the HA tagged κOR from incubation with HA antibody conjugated to Alexa Fluor 448. Expression was detected in cells transfected with the HA-tagged κOR but not the empty vector control. 80X zoom; bar = 50 mm. Results are shown for representative experiments of 3 performed.

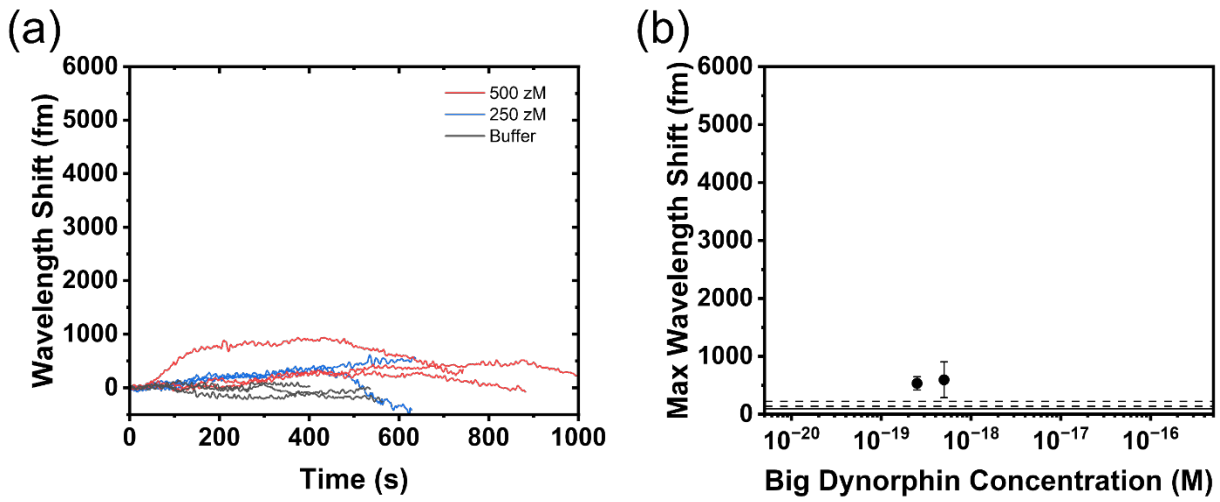

Fig. S10. (a) Wavelength shift as 250 zM and 500 zM Big Dynorphin (MW: 3982 Da) was injected into the fluidic chamber containing a κOR-lipid functionalized microtoroid. (b) The maximum wavelength shift for 250 zM and 500 zM Big Dynorphin A. Data shows the mean ±1SD from 3 independent repeats. Dashed lines show the 1SD and 3SD from the buffer mean.

Lyophilized Big Dynorphin peptide was purchased from Phoenix Pharmaceuticals, Inc. (Cat# 021-01) and solubilized in the same buffer as DynA 1-13. Wavelength shift was measured as big dynorphin was injected into the fluidic chamber containing a κOR-lipid functionalized microtoroid. The response from Big Dynorphin at zeptomolar levels is less than for DynA 1-13, which could be due to the big dynorphin molecule having slightly lower binding affinity than DynA 1-13.[3]

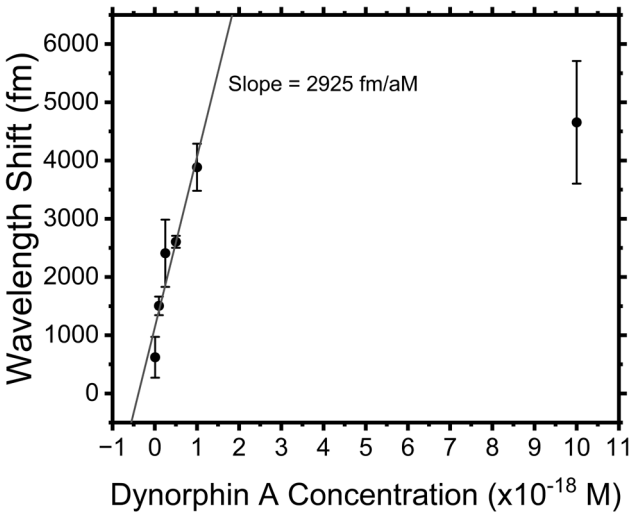

Fig. S11. Linear sensor response near the limit of detection. Whiskers show ±SD of the data.

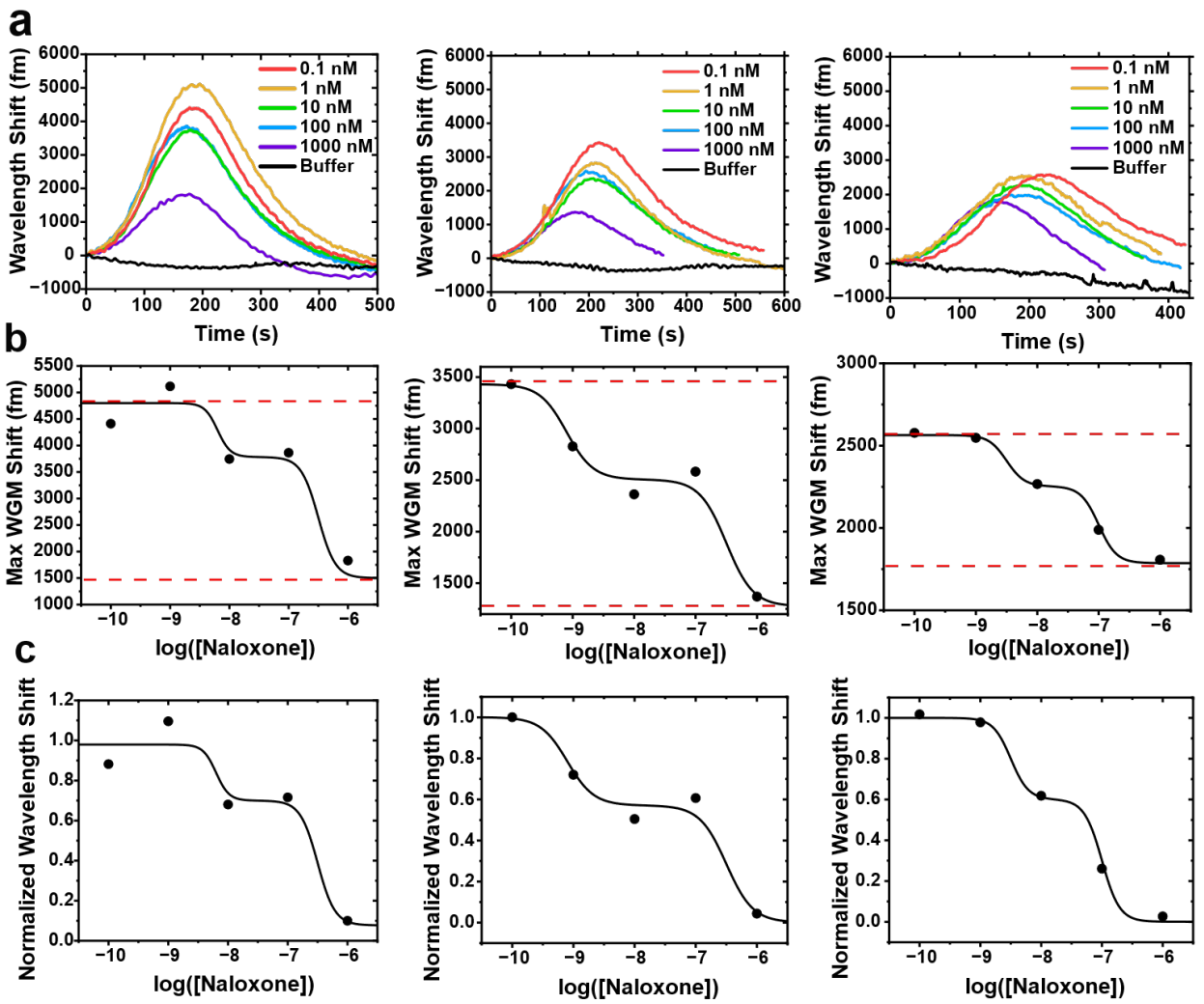

Fig. S12. (a) Wavelength shift from three repeated Naloxone/DynA 1-13 competitive binding experiments. Legend shows the naloxone concentration which was spiked with 10 nM DynA 1-13. (b) The competitive binding curve fitted with a two-site competitive binding model. The red dashed lines indicate the upper and lower asymptotes from the fit. (c) The competitive binding curves normalized using their upper and lower asymptote values from (b).

Figure S12 shows the competitive binding curves constructed from the max wavelength shifts of repeated Naloxone/DynA 1-13 competitive binding experiments. Variations in the magnitude of the wavelength shift could be due to variance in the final concentration of κOR in the lipid functionalized toroid. The upper and lower asymptotes from the fitting (red dashed lines in Fig. S12b) were taken and used to normalize the max wavelength shifts using Eqn. S2:

$$Y_{norm}(x) = \frac{Y(x) - Y_{lower}}{Y_{upper} - Y_{lower}}$$

Figure S12c shows the normalized competitive binding curve for each repeated experiment.

Constructing Binding Curves. The binding curves were constructed by plotting the peak value vs. their respective ligand concentration. The dissociation constant, K_d, was determined by fitting the peak values with the Hill-Waud model, which takes into account binding cooperativity and multiple binding sites by introducing the Hill coefficient, n[4,5]:

$$F(x) = Y_{lower} + (Y_{upper} - Y_{lower}) \frac{x^n}{K_d^n + x^n}, \quad (S1)$$

where Y_{lower} is the lower limit (fm), Y_{upper} is the upper limit (fm), x is the ligand concentration (M), K_d is the dissociation constant (M), and n is the Hill coefficient of cooperativity.

To account for experimental variations, the peak values for each experiment were normalized using the upper and lower limits from the fit curve:

$$Y_{norm}(x) = \frac{Y(x) - Y_{lower}}{Y_{upper} - Y_{lower}} \quad (S2)$$

Where $Y(x)$ is the peak value to be normalized as a function of concentration x, Y_{lower} is the lower limit of the fit curve (fm), and Y_{upper} is the upper limit of the fit curve (fm).

The inhibition constant, K_i, of naloxone was calculated from the IC_{50} by fitting the competitive binding curve with a two-site competitive binding model:

$$Part1 = \frac{P}{(1 + (IC50hi/x)^{h1})}$$

$$Part2 = \frac{(1 - P)}{(1 + (IC50lo/x)^{h2})}$$

$$Y = Part1 + Part2 \quad (S3)$$

where P is the fraction of high affinity binding sites for the competitor. *IC50hi* and *IC50lo* are the high and low IC50 values, respectively. *h1* and *h2* are the Hill slopes for the high and low IC50 values.

and the K_i was calculated from the IC50 using the equation:[6]

$$K_i = \frac{IC_{50}}{1 + \frac{R}{K_d}}, \quad (S4)$$

where R is the fixed Dynorphin A concentration (10 nM). K_d is characterized in Fig. 4d and is 3.1 nM.

The limit of detection (LOD) was determined as the lowest concentration analyte likely to be discernable from the buffer sample and was estimated using the equation:[7]

$$F_{LOD} = \overline{F_{blank}} + 3\,\sigma(F_{blank}), \quad (S5)$$

where $\overline{F_{blank}}$ is the mean signal from blank samples and $\sigma(F_{blank})$ is the standard deviation of the signal from 3 blank samples. The blank values were determined by taking the peak value from the wavelength shift of triplicate buffer injections in the LOD experiment (Fig. 5). The LOD is then the concentration where the calibration response curve intercepts F_{LOD} in Fig. 5b.

The limit of quantification (LOQ) is an estimate of the lowest concentration of analyte that can be reliably detected and quantified within some predefined measure of uncertainty and can be estimated using the equation:[8]

$$F_{LOQ} = \overline{F_{blank}} + 10\,\sigma(F_{blank}) \quad (S6)$$

Again, the LOQ is the concentration where the calibration response curve intercepts the F_{LOQ} value in Fig. 5b.

Data Acquisition. The microtoroid resonance frequency was tracked using the top-of-fringe locking function from a Toptica Digilock 110. The Digilock voltage output was connected to the laser's frequency modulation input and an analog voltage data acquisition card (DAQ) (National Instruments PCI-4461, Austin, TX, USA). The Digilock modulates the laser's frequency with a small amplitude 2 kHz sine wave and generates an error signal. As the microtoroid's resonance frequency changes, the Digilock compensates by sending a voltage signal to the laser's frequency modulation input which is also recorded by the DAQ card.

Data Processing. Typical sources of noise (e.g., electrical noise at 60 Hz) are filtered out in the Fourier domain. Finally, a median filter is used to smooth the data. The parameters from dose-response curves, competitive binding curves and statistical analysis were calculated using OriginPro 2023. Error bars show the standard error from 3-4 different experiments.

Supplementary References

1. Calmet, P., De Maria, M., Harté, E., Lamb, D., Serrano-Vega, M., Jazayeri, A., Tschammer, N. & Alves, I. D. Real time monitoring of membrane GPCR reconstitution by plasmon waveguide resonance: on the role of lipids. *Sci Rep* **6**, 36181 (2016).
2. Locatelli-Hoops, S., Yeliseev, A. A., Gawrisch, K. & Gorshkova, I. Surface plasmon resonance applied to G protein-coupled receptors. *Biomed Spectrosc Imaging* **2**, 155–181 (2013).
3. Merg, F., Filliol, D., Usynin, I., Bazov, I., Bark, N., Hurd, Y. L., Yakovleva, T., Kieffer, B. L. & Bakalkin, G. Big dynorphin as a putative endogenous ligand for the κ-opioid receptor. *Journal of Neurochemistry* **97**, 292–301 (2006).
4. Worstell, N. C., Krishnan, P., Weatherston, J. D. & Wu, H.-J. Binding Cooperativity Matters: A GM1-Like Ganglioside-Cholera Toxin B Subunit Binding Study Using a Nanocube-Based Lipid Bilayer Array. *PLoS One* **11**, (2016).
5. Lin, H., Kitova, E. N. & Klassen, J. S. Measuring Positive Cooperativity Using the Direct ESI-MS Assay. Cholera Toxin B Subunit Homopentamer Binding to GM1 Pentasaccharide. *J. Am. Soc. Mass Spectrom.* **25**, 104–110 (2014).
6. Hulme, E. C. & Trevethick, M. A. Ligand binding assays at equilibrium: validation and interpretation. *British Journal of Pharmacology* **161**, 1219 (2010).

7. Achtsnicht, S., Neuendorf, C., Faßbender, T., Nölke, G., Offenhäusser, A., Krause, H.-J. & Schröper, F. Sensitive and rapid detection of cholera toxin subunit B using magnetic frequency mixing detection. *PLOS ONE* **14**, e0219356 (2019).
8. Zorn, M. E., Gibbons, R. D. & Sonzogni, W. C. Evaluation of Approximate Methods for Calculating the Limit of Detection and Limit of Quantification. *Environ. Sci. Technol.* **33**, 2291–2295 (1999).